Research article **Open Access**

Kaung-Jay Peng, Chun-Lung Wu, Yung-Hsiang Lin, Hwai-Yung Wang, Chih-Hsien Cheng, Yu-Chieh Chi and Gong-Ru Lin*

Saturated evanescent-wave absorption of few-layer graphene-covered side-polished single-mode fiber for all-optical switching

DOI 10.1515/nanoph-2016-0182
Received November 16, 2016; revised January 15, 2017; accepted January 24, 2017

Abstract: Using the evanescent-wave saturation effect of hydrogen-free low-temperature synthesized few-layer graphene covered on the cladding region of a side-polished single-mode fiber, a blue pump/infrared probe-based all-optical switch is demonstrated with specific wavelength-dependent probe modulation efficiency. Under the illumination of a blue laser diode at 405 nm, the few-layer graphene exhibits cross-gain modulation at different wavelengths covering the C- and L-bands. At a probe power of 0.5 mW, the L-band switching throughput power variant of 16 μW results in a probe modulation depth of 3.2%. Blue shifting the probe wavelength from 1580 to 1520 nm further enlarges the switching throughput power variant to 24 mW and enhances the probe modulation depth to 5%. Enlarging the probe power from 0.5 to 1 mW further enlarges the switching throughput power variant from 25 to 58 μW to promote its probe modulation depth of up to 5.8% at 1520 nm. In contrast, the probe modulation depth degrades from 5.1% to 1.2% as the pumping power reduces from 85 to 24 mW, which is attributed to the saturable absorption of the few-layer graphene-based evanescent-wave absorber. The modulation depth at wavelength of 1550 nm under a probe power of 1 mW increases from 1.2% to 5.1%, as more carriers can be excited when increasing the blue laser power from 24 to 85 mW, whereas it decreases from 5.1% to 3.3% by increasing the input probe power from 1 to 2 mW to show an easier saturated condition at longer wavelength.

Keywords: graphene; all-optical switching; saturated evanescent-wave absorption.

1 Introduction

Recently, many types of graphene-based broadband optical modulator have been developed by various research groups [1–8]. The waveguide-type electroabsorption modulator (EAM) was demonstrated by Liu et al. [1]. High modulation speed (>1 GHz), moderate drive voltage, low energy consumption, and broadband operation (1.35–1.6 μm) are feasible; however, the coupling loss of up to 14.6 dB between the optical fiber and waveguide-type modulator is a drawback toward practical application [2]. Other kinds of graphene-based reflective-type EAMs were also developed [3]. The graphene- and ring-type electrodes are made on the top of a silver film coated on a sapphire substrate. The silver film serves as both the back electrode and the reflected mirror. The 3 dB bandwidth of this reflective-type graphene-based EAM is 154 MHz with a modulation depth of 4% at a bias of 4 V. With a small insertion loss (<3%), long active region, and uniform modulation depth (0.001–100 MHz), this device exhibits better performance toward future applications in optical communication fields. Later on, the transmission-type graphene EAM with very similar configuration to the reflective-type one is also explored to operate at THz regime, which provides a modulation depth of up to 15% under a bias of 50 V at 570 GHz with a smaller 3 dB bandwidth of 20 kHz than those in aforementioned demonstrations. Although the high carrier mobility of graphene can facilitate the enhanced electrical-to-optical throughput when performing the EAM, the practical graphene-based EAMs still exhibit the modulation speed at ~1 GHz due to RC constant limit [9].

***Corresponding author: Gong-Ru Lin,** Graduate Institute of Photonics and Optoelectronics, Department of Electrical Engineering, National Taiwan University (NTU), 1, Roosevelt Road Sec. 4, Taipei 10617, Taiwan R.O.C., e-mail: grlin@ntu.edu.tw. http://orcid.org/0000-0003-2061-1282
Kaung-Jay Peng, Chun-Lung Wu, Yung-Hsiang Lin, Hwai-Yung Wang, Chih-Hsien Cheng and Yu-Chieh Chi: Graduate Institute of Photonics and Optoelectronics, Department of Electrical Engineering, National Taiwan University (NTU), Taipei, Taiwan R.O.C.

All-optical modulation is a direct technique to prevent the bottleneck of RC constant limit. Graphene-based all-optical modulators demonstrate the ultrahigh signal modulation using the saturable absorption of graphene [9–12], which is a property that the optical absorption is reduced under intensive optical excitation. The saturable absorption of graphene with fast carrier response time (~200 fs) makes graphene a nice candidate to generate ultrahigh optical modulation; this unique characteristic is also used to produce ultrashort laser pulse [13–15]. In addition, low incident optical intensity is sufficient to operate the graphene-based optical modulator due to the low saturation intensity of graphene [16, 17], and the damage threshold of graphene is much larger than its saturation intensity [18, 19]. Consequently, the graphene-based all-optical modulator becomes a robust device in practical application. Liu et al. covered a microfiber surface with polydimethylsiloxane-supported graphene to demonstrate all-optical modulation. The evanescent-wave interacts with graphene to provide the maximal modulation depths of 5 and 13 dB for single-layer and bilayer graphene, respectively [11]. Li et al. reported the all-optical modulation using a graphene-clad microfiber with the modulation depth of 38% and a response time of ~2.2 ps. For all-optical modulation with the covered graphene, the available modulation bandwidth can be beyond 200 GHz [12, 20]. Recently, Sun et al. also used graphene to perform all-optical, electro-optical, thermo-optical, and magneto-optical modulations [20]. In particular, the graphene-based wavelength conversion of non-return-to-zero data format at 10 Gbit/s was also demonstrated, achieving the conversion efficiency and wavelength tunability of –27 dB and 12 nm, respectively [20]. As the signal extinction ratio is dominated by optical absorption in graphene, and the modulation speed is affected by the carrier relaxation time of graphene, the quality of graphene is an important factor to the performance of optical modulator. Preserving high-quality graphene without damage during the fabrication process has a great impact on the graphene-based all-optical modulator. Nevertheless, the wavelength dependence of such an all-optical modulation functionality in graphene has yet to be completely investigated.

In this work, the few-layer graphene-covered side-polished single-mode fiber (SMF) is employed as an optical evanescent-wave switch to provide the all-optical switching element for near-infrared cross-wavelength data converter. A novel growth method is proposed to fabricate graphene on ultrathin Ni film and then chemically transfer to the side-polished SMF surface through the lift-off process. The switching power variant of the cross-wavelength data converter is investigated by injecting different probe wavelengths. The wavelength-dependent saturation phenomenon on the all-optical modulation depth is observed and characterized.

2 Materials and methods

To perform the all-optical modulation of the few-layer graphene-coated SMF, a side-polished fiber with 2 cm exposed length was mounted in a glass holder initially. The proposed method is to synthesize the few-layer graphene on ultrathin Ni film on glass and then the Ni film is etched off to transfer the few-layer graphene onto the surface of side-polished fiber [21]. First, the ultrathin Ni film-coated glass substrate was placed in hydrogen-free plasma-enhanced chemical vapor deposition (PECVD) chamber at 550°C for few-layer graphene synthesis. The active gases inserted into the PECVD chamber were methane and argon with a flow rate of 3 and 200 sccm, respectively. A relatively low gas ratio of methane to argon contributes to the slow-rate carbon precipitation, which facilitates the well control of graphene layer number [22]. Such a temperature is below the melting point of glass, which would induce limited imperfections during the growth of few-layer graphene. Then, the lift-off process induced by the chemical etching of Ni film was performed at room temperature in the environment of $FeCl_3$ solution, which was kept as slow as possible to protect the few-layer graphene by greatly diluting the concentration of etching solution (Figure 1). In this way, the few-layer graphene floated on the deionized water surface after the lift-off remains flattened without any corrugation or folded damage before transferring onto the side-polished fiber [23]. The side-polished fiber was dipped into deionized water to scoop up the floated few-layer graphene, which did not risk any damages, as no physical or chemical process was performed at this stage. After diluting the $FeCl_3$ solution by injecting deionized water, the few-layer graphene was transferred onto the side-polished fiber device. In this work, Ni was introduced as a different metallic catalyst membrane in addition to Cu for the synthesis of graphene. The few-layer graphene can also be synthesized on the Ni substrate at critical phase transition temperature of the Ni/C alloy. Before the formation of few-layer graphene on Ni film, numerous C atoms are initially dissolved into Ni film to form the NiC alloy. Subsequently, these buried carbon atoms are desorbed to the Ni surface by

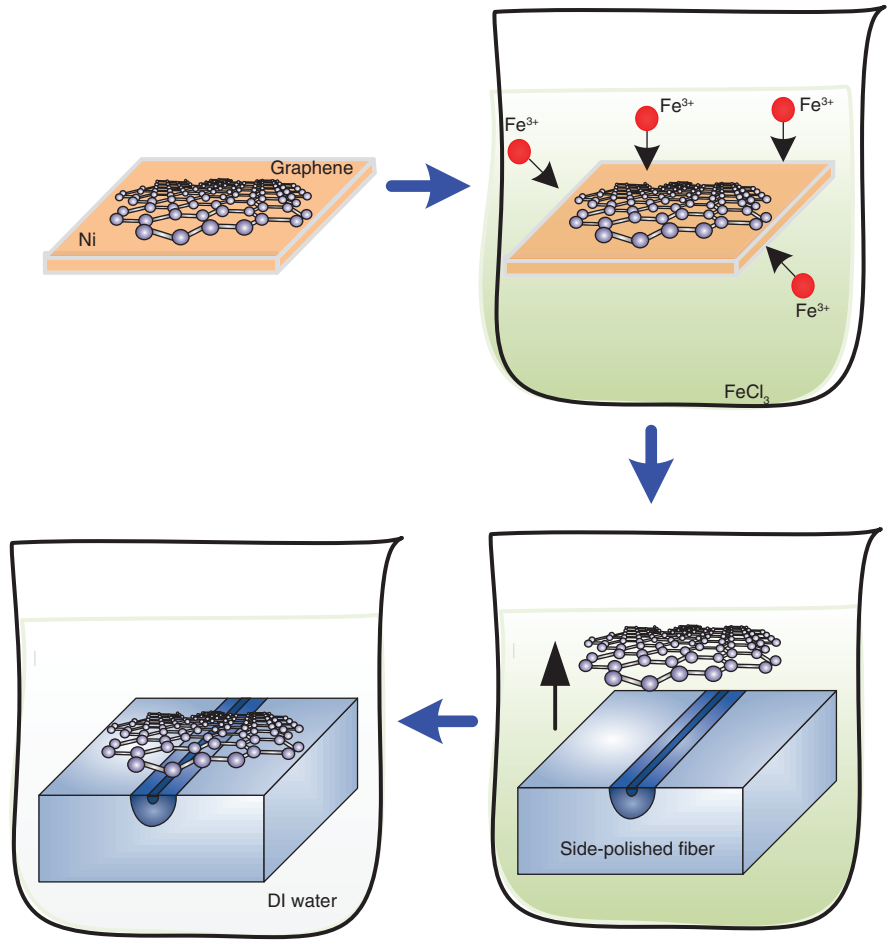

Figure 1: Solution process of few-layer graphene transferred from Ni substrate onto the side-polished SMF.

gradually cooling the Ni film to a temperature below the phase transition point. Compared to the Cu film, the slow reduction of few-layer graphene on Ni film can be obtained under hydrogen-free conditions at a relatively low temperature [22]. In addition, the lattice constant of graphene (0.246 nm) is very close to the lattice constant of hexagonally close-packed Ni (0.249 nm). Such a similarity also helps to avoid the out-of-plane buckling phenomenon during synthesis.

Figure 2 demonstrates the measuring system for analyzing the all-optical switching effect of few-layer graphene-coated side-polished fiber. A continuous-wave GaN blue laser diode (wavelength at 405 nm) was focused into a rectangular pattern by a cylindrical lens (focal length, $f = 15.4$ nm), which was served as the pump source and illuminated on the few-layer graphene-coated side-polished SMF. Simultaneously, a continuous-wave tunable laser as the probe beam was amplified by an erbium-doped fiber amplifier (EDFA). The injected wavelengths of the probe beam were 1520, 1550, and 1580 nm, respectively. The transmitted probe beam was collected by a power meter.

3 Results and discussion

Figure 3A shows the Raman scattering spectrum of the hydrogen-free few-layer graphene. Among the observed spectral components, the sp^2 orbit of carbon atoms in the C-C bond of graphene induces the G-band peak at 1582.5 cm^{-1}, the peak located at 1350 cm^{-1} denotes as the D-band related to structural defects in graphene, whereas another peak at 2700 cm^{-1} defines the 2D band induced by the zone-boundary phonons. In general, the peak ratio between G and 2D bands may be treated as preliminary data correlating well with the layer number of graphene. When decreasing the number of graphene layers, the 2D-band Raman scattering peak is increased accordingly. More accurately, it is trusted that the variation on

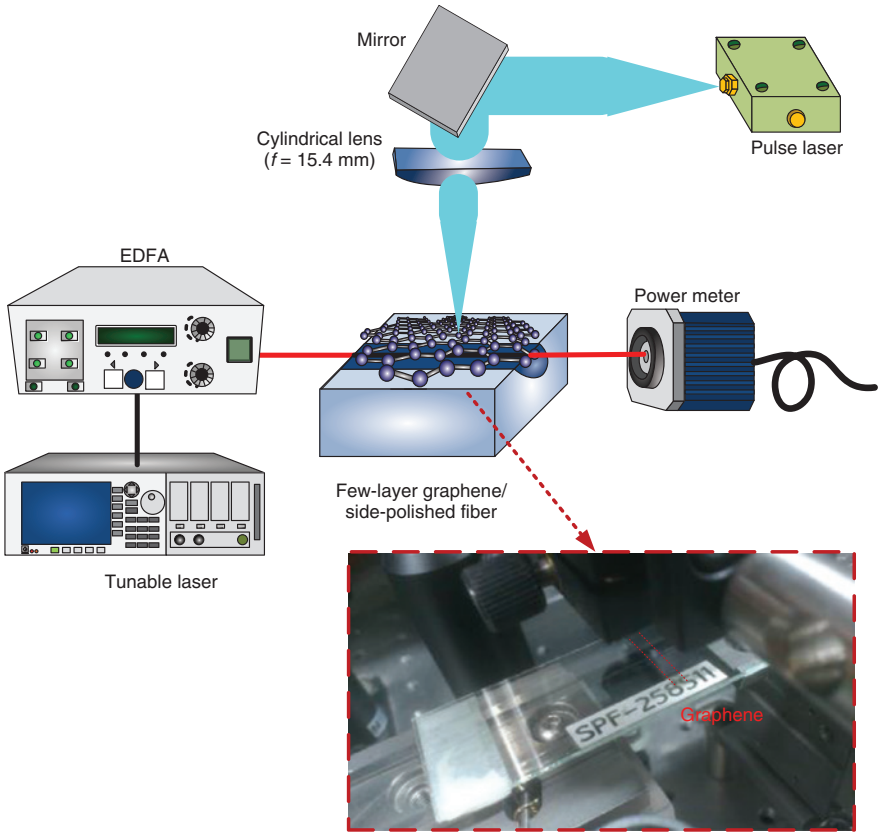

Figure 2: Schematic diagram of measuring system for analyzing the all-optical switching effect of the few-layer graphene side-polished fiber.

the number of the graphene layer affects the shift of the G-band Raman scattering shift. The relationship between the number of the graphene layer and the shift of the G-band peak can be described by [24]

$$\omega_{G,\,\text{graphene}}(\text{n}) = \omega_{\text{G, graphite}} + \frac{5.5}{\text{n}} = 1581.6 + \frac{5.5}{\text{n}}, \quad (1)$$

where $\omega_{\text{G, graphene}}(\text{n})$ denotes the wavenumber of the G-band Raman scattering peak for the graphene, $\omega_{\text{G, graphite}}$ denotes the wavenumber (1581.6 cm^{-1}) of the G-band Raman scattering peak for the graphite, and n denotes the layer number of the graphene. In our case, the number of the graphene layer is evaluated as 6–7 as the G-band Raman scattering peak shifts to 1582.5 cm^{-1}. Moreover, the peak ratio between D and G bands also provides the information of structural defects within the graphene layer [22]. Vacancy and distortion defects could be formed in graphene during its synthesis upon the ultrathin Ni film without hydrogen passivation; however, carbon atoms dissolved into and desorbed from the Ni film can be regularly reduced to graphene with slowly and smoothly cooling

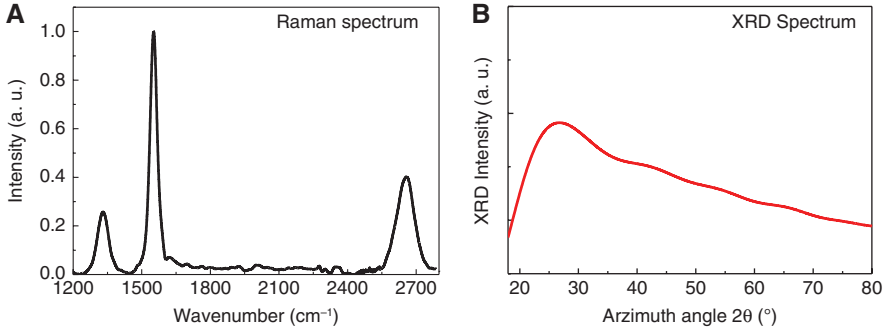

Figure 3: (A) Raman scattering spectrum and (B) XRD spectrum of few-layer graphene synthesized by hydrogen-free PECVD to observe the layer number and crystallinity of the few-layer graphene.

down the substrate temperature below the phase transition point. With this method, the defects in graphene can be minimized to result in a Raman scattering peak ratio of $I_D/I_G < 0.3$. As evidence, Figure 3B exhibits the X-ray diffraction (XRD) spectrum of the hydrogen-free PECVD synthesized few-layer graphene reduced from the Ni host membrane. The XRD peak for the few-layer graphene is located at 21°, which is close to the (002)-oriented graphene nanosheets with an azimuth angle of 23.6° [25]. The measured XRD peak is slightly smaller than the reference because the tensile strain is induced by the aforementioned defects generated in the graphene film.

Under a probe power of 0.5 mW, the switching response and the modulation depth of the few-layer graphene-coated side-polished SMF exposed to the pumped laser with different powers and wavelengths are shown in Figure 4A and B. The modulation depth is defined as the ratio of the maximal power variation to the input probe power. At pumping power of up to 85 mW, the switching power variant (*DDP*) can be 15–25 μW at a wavelength between 1520 and 1580 nm. The corresponding modulation depths (defined as *DDP*/probe power) for probe wavelengths at 1520, 1550, and 1580 nm are 5%, 3.8%, and 3.2%, respectively. The modulation depth increases with shortening the wavelength of laser because there are more states available at higher energy band of few-layer graphene (Figure 4C) [13, 14].

In addition, the modulation depth also increases with the power of pumped laser. Taking the wavelength of 1550 nm laser for example, the modulation depth is increased from 1.4% to 3.8% when enlarging the laser power from 24 to 85 mW. As the pump laser intensity increases, more carriers would be excited to the upper states to saturate the absorption of few-layer graphene such that the evanescent wave can no more excite other carriers. Most probe photons are unavailable to induce more free carrier absorption in this case. Therefore, the modulation depth of few-layer graphene-based all-optical switch shows larger modulation depth by pumping it at a shorter wavelength. In addition, the power of continuous-wave laser-based pump is too low to induce a nonlinear effect. Under the same pumping condition with a different modulation, the switching response and the modulation depth of the probe can still be improved with enlarging probe power (Figure 5B and C). By increasing the probe to 1 mW, the switching throughput *DDP* can be enlarged from 46 to 58 μW as the probe wavelength blue shifts from 1580 to 1520 nm, which gives rise to the enhanced modulation depth from 4.6% to 5.8% accordingly. The modulation depth becomes larger with increasing the probe

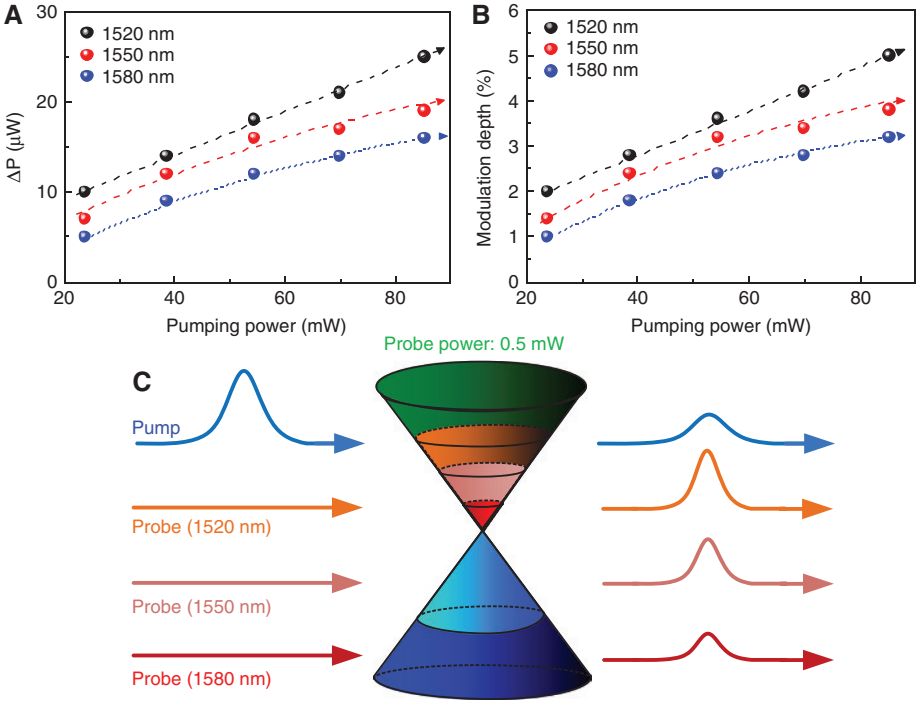

Figure 4: (A) Switching response and (B) modulation depth of few-layer graphene all-optical switcher with different probe wavelengths (probe power of 0.5 mW) and (C) schematic diagram of pump-probe analysis for performing the all-optical switching in few-layer graphene with intensive pump beam and weak probe beam at different wavelengths.

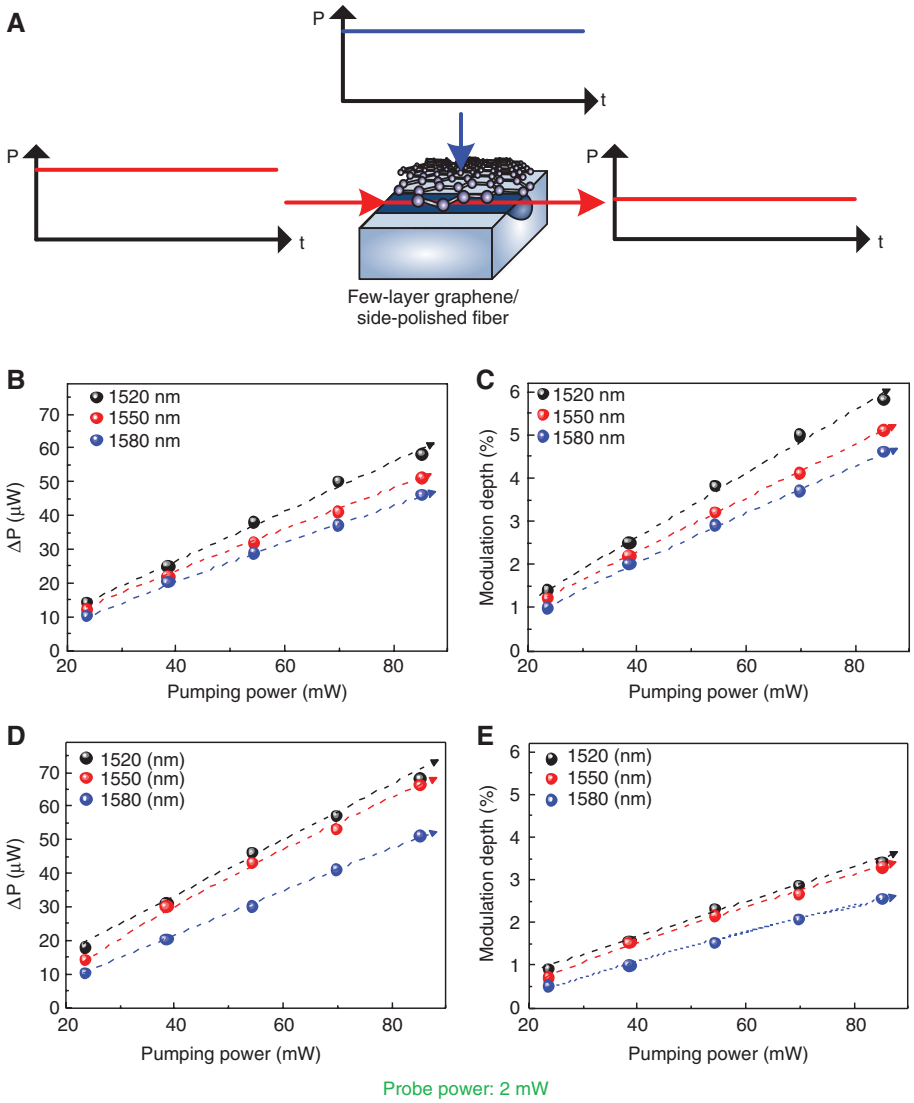

Figure 5: (A) Schematic of the pump-probe system, (B) switching response and (C) modulation depth of few-layer graphene all-optical switcher with different probe wavelengths (probe power of 1 mW), and (D) switching response and (E) modulation depth of few-layer graphene all-optical switcher with different probe wavelengths (probe power of 2 mW).

power as the increasing input power also increases the intensity of the evanescent wave, wherein more carriers can be excited to the upper states to saturate the absorption faster than ever. Figure 5D clearly reveals that the optical absorption of few-layer graphene is further saturated when increasing the probe power to 2 mW under same pumping condition, which slightly increases the switching throughput *DDP* from 51 to 68 μW as the probe wavelength blue shifts from 1580 to 1520 mW to enlarge the up-transition energy of pumping photons. As shown in Figure 5E, the modulation depths are decreased to 3.4%, 3.3%, and 2.55% corresponding to the shift of probe wavelengths to 1520, 1550, and 1580 nm, respectively. It indicates that the occupation of energy states is saturated and the absorption of evanescent wave is forbidden at a probe power of 2 mW.

From these results, it is realized that probing at longer wavelength would experience a smaller change on the transient transmission power and the saturation behavior on modulation depth occurs with increasing the pumping power as well. Such a modulation depth saturation is mainly attributed to the lower density of states for the few-layer graphene at such wavelength. As all the states at smaller energy are almost filled at 1 mW, which suffers from significant saturation effect such that larger pumping fails to implement higher modulation depth. The saturating trend on the probe power variation becomes less significant as the pumping is sufficiently large to saturate all

states, and the density of incoming probe photons is well beyond the density of states simultaneously. To explain such a saturated modulation depth behavior in principle, one needs to consider that, when graphene is photoexcited, both the intraband and interband transitions would occur as the major interactions between the conical conduction and valence bands to change its optical conductivity, as described by

$$\sigma(\omega)=\sigma_{\text{intra}}(\omega)+\sigma_{\text{inter}}(\omega), \tag{2}$$

where $\sigma_{\text{intra}}(\omega)$ is the optical conductivity for intraband transition, $\sigma_{\text{inter}}(\omega)$ is the optical conductivity for interband transition, and ω is the angular frequency of the photon. The optical absorption determined by the intraband transition at long wavelength can be described by the Drude model as [26]

$$\sigma_{\text{intra}}(\omega)=\sigma_o(E_{\text{F}})\left(\frac{8k_BT}{\pi\hbar}\right)\left(\frac{1}{\omega^2\tau+1/\tau}\right)\ln(e^{-E_{\text{F}}/2k_{\text{B}}T}+e^{E_{\text{F}}/2k_{\text{B}}T}), \tag{3}$$

where $\sigma_o(E_{\text{F}})$ denotes the original optical conductivity, τ is the momentum scattering time of carriers, E_{F} is the Fermi energy of electron, k_{B} the Boltzmann constant, e is the electron charge, $\hbar$ is the reduced Plank constant, ω is the optical frequency and T is the effective carrier temperature. In contrast, interband transition usually occurs in short wavelength range (infrared and visible) to provide an optical conductivity as [27]

$$\sigma_{\text{inter}}(\omega)=\frac{\sigma_o}{2}\left[\tanh\left(\frac{E_{\text{photon}}+2E_F}{4k_BT}\right)+\tanh\left(\frac{E_{\text{photon}}-2E_F}{4k_BT}\right)\right], \tag{4}$$

where σ_o denotes the optical conductivity of undoped graphene at $E_{\text{F}}=0$ as $e^2/4\hbar$.

In our case, the graphene sandwiched between two media of top air with its relative permittivity of one and bottom oxide with its relative permittivity of two is considered, which leads to a transmittance under normal incidence derived as [27]

$$\text{T}(\omega)=\sqrt{\frac{\varepsilon_{\text{oxide}}}{\varepsilon_{\text{air}}}}\frac{4(\varepsilon_{air}\varepsilon_0)^2}{\left|(\sqrt{\varepsilon_{\text{air}}\varepsilon_{\text{oxide}}}+\varepsilon_{\text{air}})\varepsilon_0+\sqrt{\varepsilon_{\text{air}}}\sigma(\omega)/c\right|^2}, \tag{5}$$

which is estimated as $T(\omega)=0.982-0.82\text{s}[\sigma(\omega)/c]$. Assuming the simplest case in vacuum, the transmittance of single-layer graphene can be approximated as $T=1-\pi\alpha$ with $\alpha=e^2/2\varepsilon_0\text{ch}$, whereas the transmittance of bilayer graphene needs to be calibrated as $T=1-\pi\alpha f_2(\omega)$ with the factor of $f_2(\omega)$ given by

$$f_2(\omega)=\frac{E_{\text{photon}}+2E_{\text{hopping}}}{2(E_{\text{photon}}+E_{\text{hopping}})}+\frac{\theta(E_{\text{photon}}-E_{\text{hopping}})}{(E_{\text{photon}}/E_{\text{hopping}})^2}+\frac{(E_{\text{photon}}-2E_{\text{hopping}})\theta(E_{\text{photon}}-2E_{\text{hopping}})}{2(E_{\text{photon}}-E_{\text{hopping}})}, \tag{6}$$

which clearly indicates the wavelength dependence of the transmittance as the layer number of graphene increases. That is, the wavelength-dependent phenomena on both the variations of the throughput power and modulation depth can be caused by the bilayer or multilayer geometry of the graphene sample synthesized by ourselves. In general, the transmittance as well as the modulation efficiency of the waveguide covered by graphene should be irrelevant to the probing wavelength if the Fermi level is unchanged or if the pump remains relatively weak during the pump-probe analysis. Nevertheless, the intense pump should provide a significant band filling effect such that the aforementioned parameters concurrently change as well.

As expected, the optical conductivity is correlated with the voltage-dependent Fermi level of few-layer graphene. The operating principle of the all-optical switch based on optically illuminating the few-layer graphene-coated side-polished SMF is shown in Figure 6A and B. As the all-optical modulation is dominated by changing the absorption coefficient of graphene with the evanescent wave of pump laser when passing through the SMF core, the evanescent wave outside the side-polished SMF would be absorbed by the coated graphene layer to give an "off" state under the all-optical switching process at initial stage. As the evanescent wave of pump laser excitation fills out the excited state of the graphene to saturate its absorption, the evanescent wave can directly pass through

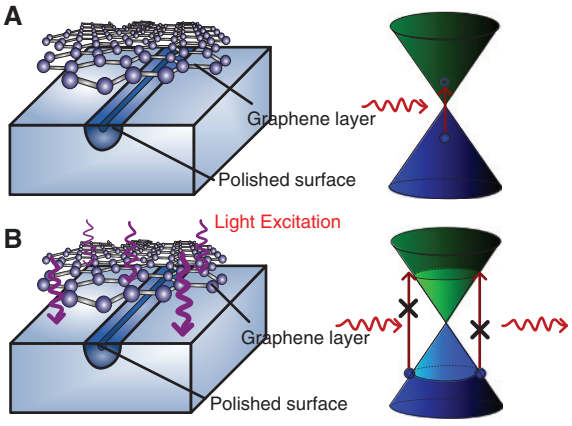

Figure 6: Schematic diagram of photon absorption in graphene (A) with and (B) without intensive light excitation.

the graphene layer without suffering from the absorption to excite further carriers. When turning off the pump laser, this phenomenon ceases and eventually results in the "on" state of the incoming probe light. In the case of continuous-wave laser pumping, there will be much lower evanescent-wave intensity to induce the absorption saturation within the covered graphene layer compared to the case with pulsed laser of higher intensity. Hence, the continuous-wave laser-based pump provides weaker evanescent wave and exhibits less impact to the variation of probe intensity. In addition, the few-layer graphene also provides a smaller change of saturation absorption than the monolayer graphene. This explains the reason for the smaller modulation depth of the few-layer graphene-covered side-polished fiber modulator compared to previous works with better performance. Some remarkable references are summarized as evidence of the aforementioned discussion in previous works. For example, Li et al. demonstrated all-optical modulation using a graphene-clad microfiber all-optical modulator. The pumping laser was a femtosecond-degree pulsed laser with peak power intensity of ~GW/cm^2. The achieved modulation depth was 38% [12]. In addition, Yu et al. also used a graphene-clad microfiber to investigate the all-optical intensity modulation. As the peak power of switching light at 1.06 μm increased to 1.15 W, the modulation depth of probe laser at 1.55 μm can achieve 11.5% [28]. Liu et al. also reported different modulation depths from a graphene-covered microfiber with single-layer and bilayer graphene [11]. In our work, the all-optical modulation using a graphene covered single-side-polished SMF is demonstrated at much lower pump intensity than others. Both the pump-induced absorption change and the interaction area of the device are less than those of the graphene-cladded microfiber (with surrounding graphene). With the use of a high-quality monolayer graphene, the modulation depth of the graphene-covered side-polished fiber can induce the all-optical modulation up to ~6%. Except for the aforementioned reasons, the structural defects induced during the lift-off transfer of the few-layer graphene from ultrathin Ni membrane to the side-polished SMF surface could also be one possible mechanism to degrade the performance of modulation efficiency.

4 Conclusion

In this work, the few-layer graphene-covered side-polished SMF is employed as an all-optical switching element at different wavelengths that covered the C- and L-bands. At a probe power of 0.5 mW, the L-band switching throughput power variant of 16 μW is observed with a modulation depth of 3.2% at a probe power of 0.5 mW. Blue shifting the probe wavelength from 1580 to 1520 nm further enlarges the switching throughput power variant to 25 μW and enhances the modulation depth to 5%. The modulation depth increases with shortening wavelength as the pumping laser at shorter wavelength can induce more free carriers to saturate the states closer to the Dirac point, which would suppress the absorption of the incoming probe power at longer wavelengths. Enlarging the probe power from 0.5 to 1 mW further enlarges the switching throughput power variant from 46 to 58 μW to promote its modulation depth up to 5.8% at 1520 nm. All the states at smaller energy are almost filled at 1 mW, which suffers from a significant saturation effect, such that larger pumping fails to implement higher modulation depth. The saturating trend on the probe power variation becomes less significant, as the pumping is sufficiently large to saturate all states, and the density of incoming probe photons is well beyond the density of states simultaneously. By further increasing the probe power of up to 2 mW under the same pumping condition, the change of switching throughput clearly decays from 68 to 51 μW when red shifting the probe wavelength from 1520 to 1580 mW, indicating that the optical absorption of few-layer graphene is easier saturated at longer wavelengths. The modulation depths are gradually decreased to 3.4%, 3.3%, and 2.55% with the probe wavelengths of 1520, 1550, and 1580 nm, respectively, owing to the finite density of states of few-layer graphene in the near Dirac-point region.

Acknowledgments: The authors thank the Ministry of Science and Technology (Taiwan, R.O.C.) and the Excellent Research Projects of the National Taiwan University (Taiwan, R.O.C.) for financially supporting this research under grants MOST-103-2221-E002-042-MY3, MOST-104-2221-E-002-117-MY3, NTU-ERP-105R89081, and NTU-ERP-105R89083.

References

[1] Liu M, Yin X, Avila EU, et al. A graphene-based broadband optical modulator. Nature 2011;474:64–7.
[2] Liu M, Yin X, Zhang X. Double-layer graphene optical modulator. Nano Lett 2013;12:1482–5.
[3] Lee C-C, Suzuki S, Xie W, Schibli TR. Broadband graphene electro-optic modulators with sub-wavelength thickness. Opt Express 2012;20:5264–9.

[4] Lu Z, Zhao W. Nanoscale electro-optic modulators based on graphene-slot waveguides. J Opt Soc Am B 2012;29:1490–6.
[5] Koester SJ, Li M. High-speed waveguide-coupled graphene-on-graphene optical modulators. Appl Phys Lett 2012;100:171107.
[6] Hao R, Du W, Chen H, Jin X, Yang L, Li E. Ultra-compact optical modulator by graphene induced electro-refraction effect. Appl Phys Lett 2013;103:061116.
[7] Polat EO, Kocabas C. Broadband optical modulators based on graphene supercapacitors. Nano Lett 2013;13:5851–7.
[8] Mohsin M, Schall D, Otto M, Noculak A, Neumaier D, Kurz H. Graphene based low insertion loss electro-absorption modulator on SOI waveguide. Opt Express 2014;22:15292–7.
[9] Luo S, Wang Y, Tong X, Wang Z. Graphene-based optical modulators. Nanoscale Res Lett 2014;10:1–11.
[10] Bao Q, Loh KP. Graphene photonics, plasmonics, and broadband optoelectronic devices. ACS Nano 2012;6:3677–94.
[11] Liu Z-B, Feng M, Jiang W-S, et al. Broadband all-optical modulation using a graphene-covered-microfiber. Laser Phys Lett 2013;10:065901.
[12] Li W, Chen B, Meng C, et al. Ultrafast all-optical graphene modulator. Nano Lett 2014;14:955–9.
[13] Bao Q, Zhang H, Wang Y, et al. Atomic-layer graphene as a saturable absorber for ultrafast pulsed lasers. Adv Funct Mater 2009;19:3077–83.
[14] Sun Z, Hasan T, Torrisi F, et al. Graphene mode-locked ultrafast laser. ACS Nano 2010;4:803–10.
[15] Lin Y-H, Yang C-Y, Liou J-H, Yu C-P, Lin G-R. Using graphene nano-particle embedded in photonic crystal fiber for evanescent wave mode-locking of fiber laser. Opt Express 2013;21:16763–76.
[16] Xing G, Guo H, Zhang X, Sum TC, Huan CHA. The physics of ultrafast saturable absorption in graphene. Opt Express 2010;18:4564–73.
[17] Lin Y-H, Yang C-Y, Lin S-F, Lin G-R. Triturating versatile carbon materials as saturable absorptive nano powders for ultrafast pulsating of erbium-doped fiber lasers. Opt Mater Express 2015;5:236–53.
[18] Martinez A, Sun Z. Nanotube and graphene saturable absorbers for fibre laser. Nat Photon 2013;7:842–5.
[19] Xiong Y, Yan L, Si J, et al. Cascaded optical limiter with low activating and high damage thresholds using single-layer graphene and single-walled carbon nanotubes. J Appl Phys 2014;105:083111.
[20] Sun Z, Martinez A, Wang F. Optical modulators with 2D layered materials. Nat Photon 2016;10:227–38.
[21] Ferrari AC, Bonaccorso F, Fal'ko V, et al. Science and technology roadmap for graphene, related two-dimensional crystals, and hybrid systems. Nanoscale 2015;7:4598–810.
[22] Peng K-J, Wu C-L, Lin Y-H, et al. Hydrogen-free PECVD growth of few-layer graphene on an ultra-thin nickel film at the threshold dissolution temperature. J Mater Chem C 2013;1:3862–70.
[23] Peng K-J, Lin Y-H, Wu C-L, et al. Dissolution-and-reduction CVD synthesis of few-layer graphene on ultra-thin nickel film lifted off for mode-locking fiber lasers. Sci Rep 2015;5:13689.
[24] Gupta A, Chen G, Joshi P, Tadigadapa S, Eklund PC. Raman scattering from high-frequency phonons in supported n-graphene layer films. Nano Lett 2006;6:2667–73.
[25] Wang G, Yang J, Park J, et al. Facile synthesis and characterization of graphene nanosheets. J Phys Chem C 2008;112:8192–5.
[26] Choi H, Borondics F, Siegel DA, Zhou SY, Martin MC. Broadband electromagnetic response and ultrafast dynamics of few-layer epitaxial graphene. Appl Phys Lett 2009;94:172102.
[27] Stauber T, Peres NMR, Geim AK. Optical conductivity of graphene in the visible region of the spectrum. Phys Rev B 2008;78:085432.
[28] Yu S, Wu X, Chen K, et al. All-optical graphene modulator based on optical Kerr phase shift. Optica 2016;3:541–4.